

Silicon Monoxide at 1 atm and Elevated Pressures: Crystalline or Amorphous?

Khalid AlKaabi,[†] Dasari L. V. K. Prasad,^{†,#} Peter Kroll,[§] N. W. Ashcroft,[‡] and Roald Hoffmann^{*,†}

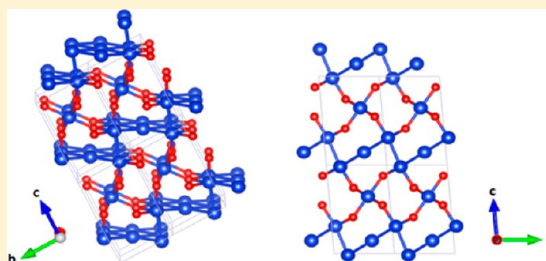
[†]Department of Chemistry and Chemical Biology, Cornell University, Ithaca, New York 14853, United States

[§]Department of Chemistry and Biochemistry, The University of Texas at Arlington, Arlington, Texas 76019-0065, United States

[‡]Laboratory of Atomic and Solid State Physics, Cornell University, Ithaca, New York 14853, United States

Supporting Information

ABSTRACT: The absence of a crystalline SiO phase under ordinary conditions is an anomaly in the sequence of group 14 monoxides. We explore theoretically ordered ground-state and amorphous structures for SiO at $P = 1$ atm, and crystalline phases also at pressures up to 200 GPa. Several competitive ground-state $P = 1$ atm structures are found, perforce with Si–Si bonds, and possessing Si–O–Si bridges similar to those in silica (SiO₂) polymorphs. The most stable of these static structures is enthalpically just a little more stable than a calculated random bond model of amorphous SiO. In that model we find no segregation into regions of amorphous Si and amorphous SiO₂. The $P = 1$ atm structures are all semiconducting. As the pressure is increased, intriguing new crystalline structures evolve, incorporating Si triangular nets or strips and stishovite-like regions. A heat of formation of crystalline SiO is computed; it is found to be the most negative of all the group 14 monoxides. Yet, given the stability of SiO₂, the disproportionation $2\text{SiO}_{(s)} \rightarrow \text{Si}_{(s)} + \text{SiO}_{2(s)}$ is exothermic, falling right into the series of group 14 monoxides, and ranging from a highly negative ΔH of disproportionation for CO to highly positive for PbO. There is no major change in the heat of disproportionation with pressure, i.e., no range of stability of SiO with respect to SiO₂. The high-pressure SiO phases are metallic.



INTRODUCTION

While SiO₂ is one of the most studied compositions of matter under high pressure,^{1–3} because of its importance to the geochemistry and geophysics of the Earth and other planets, the monoxide or suboxide, SiO, is less well known. That is quite a contrast with other monoxides of the carbon group—CO, SnO, and PbO are familiar molecules or solids. This paper explores this mystery of group 14: the apparent absence of crystalline SiO at $P = 1$ atm and higher pressures.

SiO is there. A material of approximate SiO composition can be made reproducibly enough to be sold in volume—it has found its way into technological applications.^{4,5} However, its microscopic structure remains subject to controversy; an excellent review by Schnurre, Gröbner, and Schmidt-Fetzer⁶ has a vivid Appendix with more than 80 references debating the nature of SiO. Recent studies have characterized SiO as an amorphous solid that is neither homogeneous and single-phase nor a two-phase heterogeneous mixture (of Si and SiO₂). One such comprehensive investigation, using a combination of physical techniques, argues for a heterogeneous structure that contains clusters of SiO₂ and Si surrounded by a suboxide matrix.⁷ There appear to be many atoms at Si/SiO₂ interfaces, causing composition fluctuations that are continuous, rather than abrupt.⁶ Either way, as an amorphous solid or a heterogeneous mixture, SiO is not simple in structural terms.

Interestingly, the monoxide of silicon is also the subject of astrophysical studies, because of its high interstellar abun-

dance.^{8,9,12} Diatomic SiO, well-known on Earth as a metastable molecule (the Si–O separation is 1.49 Å),⁹ has also been detected in sunspots. It was suggested that SiO¹⁰ is the initial condensate in the outflows of oxygen-rich dying stars. Some crystalline silicate grains have been observed in the dust shells around those stars at temperatures above 1000 K. There is some theoretical work on SiO nanoaggregates,¹¹ and oligomers of SiO have been detected and assessed in calculations.¹²

All monoxides in group 14, except those of silicon and germanium, are known in the pure solid phase. CO is molecular in the solid phase (even as more stable extended structures have been suggested),¹³ while SnO and PbO exist in extended structures. The known monoxides have lower magnitude negative heats of formation than the corresponding dioxides (Table 1), yet clearly persist over a significant temperature range at $P = 1$ atm and also in the presence of O₂. This indicates that the barriers to reaction with molecular oxygen to form the dioxide are high, and it encourages one to think that the metastability of hypothetical SiO (or GeO) is not an impediment to its persistence. Moreover, the high-pressure variable opens up a new perspective—could SiO (and GeO) actually be stabilized at elevated pressure?

Since SiO is not known as a pure crystalline solid, we must search for its possible structure(s). Previous calculations^{18,19}

Received: September 22, 2013

Published: February 4, 2014

Table 1. Comparison of Heats of Formation of the Monoxides and Dioxides of Group 14 in Their Most Stable States at $P = 1$ atm^a

AO	ΔH_f (kJ/mol), monoxide	AO ₂	ΔH_f (kJ/mol), dioxide
CO _(g)	-111	CO _{2(g)}	-394
SiO _(g)	-100 ^b	SiO _{2(s)} (quartz)	-911
SiO _(am)	-423 ^c		
SiO _(s)	-363 ^c		
GeO _(g)	-39 ^{b,15,16}	GeO _{2(s)} (tetragonal)	-580 ¹⁷
SnO _(s) (tetragonal)	-281 ¹⁷	SnO _{2(s)} (tetragonal)	-578 ¹⁷
PbO _(s) (tetragonal)	-219	PbO _{2(s)}	-274

^aAll the values, unless otherwise specified, were obtained from ref 14. They are rounded off to the nearest kJ/mol. ^bThe heats of formation listed in the table for SiO (first entry) and GeO are for the diatomic molecules. The diatomics are much less stable than hypothetical solids (for SiO) calculated in this paper. The source of the latter values will be given below when we discuss the enthalpic stability of the solid phases we study. ^cThis work. Hypothetical SiO solid calculated in its most stable phase at $P = 1$ atm, I, will be discussed in the text. This is a ground-state value, not at 298 K.

have in fact explored some potential structures for SiO and also GeO at $P = 1$ atm. Our search for possible crystalline SiO structures began by testing existing and calculated group 14 suboxide structures. In addition, we searched for structures using evolutionary algorithm and random search techniques. Finally, we calculated several approximants to amorphous solid SiO.

The methods used throughout are based on evolutionary and random structure searching and assessment methods coupled with density functional theory (DFT; the general approaches as well as the numerical details and computational procedures are laid out in the Theoretical Section). For crystalline choices, the strategies are quite straightforward; however, in this paper we go a step further and explore variants which we will refer to as “simulated amorphous”; these static, but plainly disordered arrangements will be described below.

Our calculations were calibrated with two silica modifications— α -quartz and stishovite. For these systems, as well as for elemental O and Si, which we need for calculations of the heats of formation, our calculations gave structures similar in detail to those known or calculated by others.^{20–22} All the enthalpies given in this paper are for ground-state structures; zero point energies (ZPEs) were not included. This might be a concern, since the ZPEs (ranging from 0.17 eV at $P = 1$ atm to 0.20 eV at 50 GPa) are comparable to the differences in enthalpy between a number of the structures. But we do not expect ZPEs to have an effect on structural choices, as they are reasonably the same for all alternative structures. Also our calibrations on some of the known forms of SiO₂ gave the order of stability known without ZPEs.

RESULTS AND DISCUSSION

SiO at 1 atm. Let us voice at the outset the obvious—SiO is going to be unstable with respect to disproportionation to SiO₂ and Si, no matter what crystal structure we predict. Si–O bonds are exceedingly strong.^{23–25} There are twice as many such Si–O bonds in SiO₂ as in SiO. We do not expect the Si–O bond energy in SiO₂ and SiO to be much different since, as will be discussed, the two materials have similar calculated Si–O bond

lengths. A consequence of the great stability of Si–O polar covalent single bonding is that Si–O–Si linkages are bound to be there in SiO structures, and their number is maximized (even as there must be Si–Si bonds as well). These Si–O–Si units are likely to vary in angle, as is found in silica structures. Finally, given the cornucopia of nearly equal in enthalpy SiO₂ structures available to us, we are likely to find not one but many nearly equal enthalpy SiO possibilities. And, as will be seen, we do.

Elements of the same group often behave in similar ways. Accordingly, we began our search for possible stable SiO phases with known solid-state structures of the monoxides of group 14 (CO, SnO, and PbO) as well as some recently calculated alternative structures of solid CO.¹³ Among these, the most thermodynamically stable candidates were obtained from the hypothetical CO structures studied earlier.¹³ Two structures with the orthorhombic symmetries *Cmcm* and *Pmma* are almost identical in energy at $P = 1$ atm. Figure 1 gives the geometry of

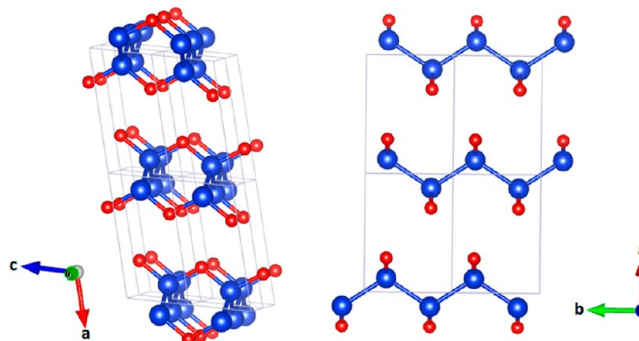


Figure 1. Ground-state *Cmcm* structure at $P = 1$ atm in two views [blue = Si, red = O].

one of these, *Cmcm*; the other one, differing by a slight shift of the 2D planes relative to each other, is shown in the Supporting Information (SI) that accompanies this paper. The slightly less stable *C2/c* and *C1* structures lie only 0.11 and 0.19 eV/SiO in enthalpy above the *Cmcm* structure, respectively.

In the orthorhombic *Cmcm* structure ($Z = 2$, Figure 1), each silicon atom is coordinated to four nearest neighbors: two Si and two O atoms. Each Si atom is bridged to the next-nearest Si by an O atom (along the *c*-axis), forming nonplanar 6-membered rings similar to those calculated for CO.¹³ These rings are not isolated but are in-turn connected along the *b*-axis into sheets by sharing Si–O–Si bonds. As reported in Table 2, calculated Si–Si and Si–O bond lengths in *Cmcm* at 1 atm are 2.41 and 1.68 Å, respectively, these being comparable in fact to the Si–Si separation in cubic diamond silicon (calculated, 2.37 Å; experimental, 2.35 Å²⁶) and Si–O in α -quartz (calculated, 1.62 and 1.63 Å; experimental,²⁷ 1.61 Å). The Si–O–Si angle is 114°, which is smaller than the one found (calculated) in α -quartz, 147° (experimental,²⁷ 144°).

From a chemical perspective, we see here immediately the essential features that distinguish SiO from CO. (1) Multiple bonding is well known in carbon chemistry, but difficult to achieve in a persistent manner in silicon chemistry.²⁸ The thermodynamically stable and kinetically persistent SiO structures will not be diatomic but extended, solid-state structures that are “saturated”, i.e., will have at $P = 1$ atm four bonds to each Si and two to O. (2) The Si–O–Si bond angle is much less resistant to opening from a tetrahedral value,

Table 2. Calculated Static and Ground-State Bond Lengths of All the Structures Analyzed in This Work, as Well as Stable SiO₂ and Si Phases at Pressures of Interest

structure	<i>P</i> (GPa)	Si–O (Å)	Si–Si (Å)
Si (cubic diamond)	0		2.37 (2.35 ²⁶) ^a
Si (hcp)	50		2.44
Si (fcc)	50		2.47
SiO ₂ (α -quartz)	0	1.62, 1.63 (1.61 ²⁷) ^a	
SiO ₂ (stishovite)	50	1.72	
<i>Cmcm</i>	0	1.68	2.41
I (<i>Cm</i>)	0	1.65–1.66	2.36–2.51
II ($\bar{I}4$)	0	1.63–1.67	2.35, 2.41
III (<i>C2</i>)	0	1.65–1.66	2.39–2.49
A (<i>P2/m</i>)	50	1.72–1.85	2.22–2.28
B (<i>Imm2</i>)	50	1.70–1.79	2.31–2.55
C (<i>Imm2</i>)	50	1.76–1.87	2.26–2.29
D (<i>P1-C2/m</i>)	50	1.70–1.80	2.31–2.55
E (<i>C2/m</i>)	50	1.70–1.78	2.36–2.55

^aExperimental values under ordinary conditions are given in parentheses.

even to 180°, than a comparable C–O–C angle. This is consistent with the wide range of such angles found in the many polymorphs of silica,²⁰ and can be seen in a comparative calculation of a model compound such as (HO)₃-E-O-E-(OH)₃, E = C, Si (calculated, 121° for C, 134° for Si). The energy to distort from this minimum in the model molecules to a linear E–O–E bond is 1.4 eV for C, 0.08 eV for Si (per formula unit).^{29,30}

A further feature of SiO relative to SiO₂ is that “deletion of oxygens” in the former (relative to the latter) must lead to the formation of some Si–Si bonds. Actually, as part of our search, we took this deletion argument seriously, by taking known quartz allotropes and deleting some oxygens from them. But no “better” structural candidates subsequently emerged.

Evolutionary and random structure searches (see the Theoretical Section) led to several phases that are more stable than the ground-state *Cmcm* structure described above at *P* = 1 atm.³¹ The most stable of these structures are labeled here as I, II, and III. The symmetry and relative stability of these phases are given in Table 3. Their structures are shown in Figures 2–4.

Table 3. Symmetry and Ground-State Enthalpy (Relative to the *Cmcm* Structure) of the Most Stable Phases at *P* = 1 atm

phase	space group	<i>Z</i> ^a	relative stability	
			in eV/SiO	in kJ/mol/SiO
I	<i>Cm</i>	8	–0.38	–37
II	$\bar{I}4$	16	–0.33	–32
III	<i>C2</i>	4	–0.23	–22

^a*Z* = number of formula units per unit cell.

Other structures with similar relative stabilities at *P* = 1 atm were also predicted and are discussed in the SI. Note that one expectation is met: there is not one, but a goodly number of competitive SiO structures, and in a way this is not that different from SiO₂.

Structure I is calculated to be the most stable phase of SiO at *P* = 1 atm. Interestingly, the structure contains nearly planar 6-membered rings consisting of four Si and two O atoms. The 6-membered rings can be seen clearly in the top view along the *a*-axis in Figure 2, where each ring is connected to eight other

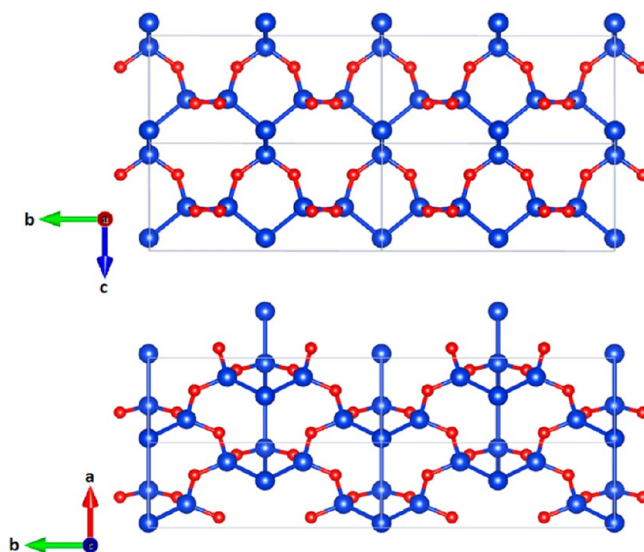


Figure 2. Ground-state structure of the crystalline form of SiO calculated to be lowest in enthalpy, I, at *P* = 1 atm. Six-membered rings can be seen along the *a*-axis (top) [blue = Si, red = O].

rings. Along the *c*-axis, the rings form ladder-like arrangements where each “step” (ring) is connected to the next via Si–Si bonds. The Si atoms are 4-coordinated, with three types of bonding environments for Si: (Si₄), (O₃Si), and (Si₂O₂). All O atoms are 2-coordinated. Along the *a*- and *b*-axes, the rings are connected with each other via Si–O–Si bonds with a bond angle of 124°.

A structure closely related to I, of *C1* symmetry, is shown in the SI (labeled as structure IV). It also contains 6-membered Si₄O₂ rings in a ladder-like arrangement, but with a different interconnection motif. One Si–O–Si unit in this structure is almost linear; such nearly linear bonds are found in one of the SiO₂ polymorphs, namely tridymite, which features a bond angle of 178–180°.³² This structure is 0.06 eV/SiO less stable than I. Note the small effect of variations in the Si–O–Si angle on structure stability; we have referred to this above.

The next competitive structure in energy, only 0.05 eV/SiO above I, is II, shown in Figure 3. This is a nicely symmetric structure ($\bar{I}4$), containing two alternating layers. Each layer is made up of three types of nonplanar rings: 10-membered rings (two different orientations) consisting of eight Si and two O atoms, 8-membered rings consisting of four Si and four O atoms, and 4-membered rings consisting of only Si atoms. The layers are connected via Si–O–Si bonds along the *c*-axis and are shifted with respect to their 2-D planes. The Si atoms have two bonding environments: (Si₃O) and (O₃Si). Oxygen atoms form Si–O–Si connections with two quite open bond angles: 145° and 161°. In the carbon world, 4-membered rings would be a harbinger of instability, but they are not for Si.

The structure of III (Figure 4), about 0.16 eV/SiO less stable than I at *P* = 1 atm, contains 4-coordinated Si atoms with four different bonding environments for Si: (Si₄), (O₃Si), with two distinct types, and (O₂Si₂). Interestingly, part of the Si sublattice forms nonlinear (zigzag) Si chains that extend along the *a*-axis. These chains are connected with each other by quartz-like units (see view along *b*-axis in Figure 4). In this structure, 8-membered rings can be identified, consisting of five Si and three O atoms (in contrast to the 12-membered rings found in α -quartz). Si–O–Si angles are 129–133°. Notable is a significant distortion from ideal tetrahedra around Si: a

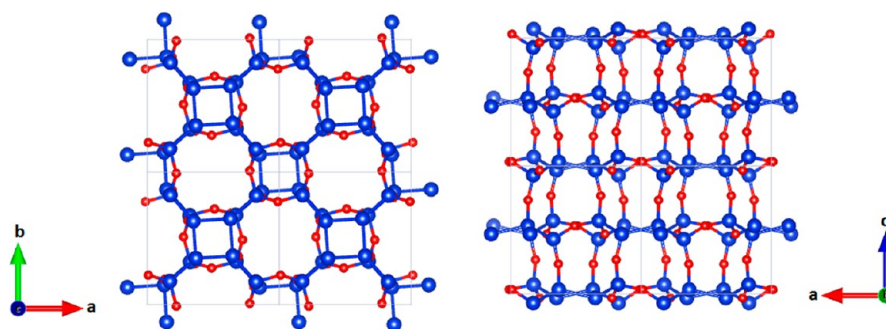


Figure 3. Ground-state structure of **II** at $P = 1$ atm. Ten-, eight-, and four-membered rings can be seen along the c -axis (left) [blue = Si, red = O].

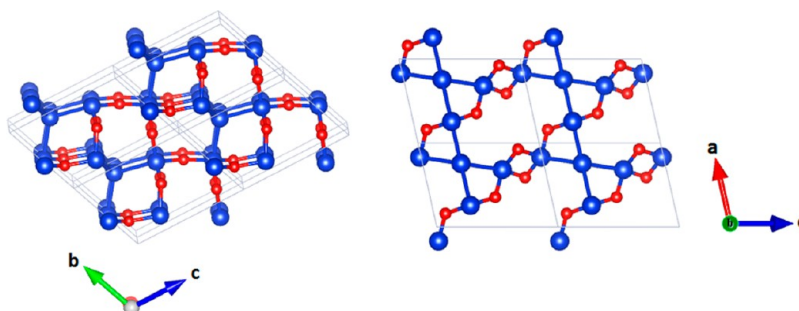


Figure 4. Ground-state structure of **III** at $P = 1$ atm. The quartz-like units connecting the Si chains can be clearly seen in the view along the b -axis [blue = Si, red = O].

maximum Si–Si–O angle of 131° occurs in Si bonded to (SiO_3), and a minimum angle of 90° in Si-coordinated Si atoms (all angles in quartz are $109 \pm 1^\circ$ ³³).

As mentioned above, some other structures have been suggested previously for crystalline SiO_2 ;¹⁸ we have also examined those. The most stable, the distorted SnO-type structure, was calculated here as 1.1 eV/SiO less stable than the structure of **I**. All the SiO structures we identified are energetically unstable with respect to disproportionation to Si and α - SiO_2 at $P = 1$ atm. We will return to the energetics of the various structures after we examine a model for amorphous and high-pressure crystalline SiO phases, to which we shortly turn.

Since it is known that the calculated relative enthalpies of SiO_2 strongly depend on the choice of the energy functional in DFT calculations,²⁰ at the suggestion of a reviewer we have also recalculated our most stable models for SiO using local density approximation (LDA) potentials. In the $P = 1$ atm region, structure **I** remains the most stable candidate. Interestingly, structure **III** is relatively stabilized with LDA potentials and becomes the second most stable structure in terms of enthalpy. Therefore, the order of stability of the $P = 1$ atm structures calculated with LDA potentials becomes $\text{I} < \text{III} < \text{II} < \text{IV}$. Table S3 in the SI compares the relative energies of the most stable structures for the GGA-PBE and LDA functional calculations.

A Model for Amorphous SiO . To test the energetic stability of our ordered structures relative to an amorphous solid (at $P = 1$ atm), we generated defect-free tetrahedral networks of amorphous SiO using a modified Wooten–Winer–Wearie algorithm,³⁴ which was used in previous work on SiCO glasses and SiO_2 .³⁵ The starting structure for the network modeling was built from a model of SiO_2 glass by depleting it of some O atoms and then rebonding the free valences. The same simple Keating-type potential as in previous studies was used.³⁶ Employing a variety of annealing procedures, we generated 42 models with 36 SiO units and

28 models with 108 SiO units. We optimized all smaller models and two of the larger models (selected by their low energy) using DFT methods described in the Theoretical Section. The principal assumption, namely that energies associated with mutual interactions can be represented at the pair level, is not without its difficulties. However, the move to DFT-based energies in the refinement process should ameliorate these somewhat.

Interestingly, the most stable amorphous model is actually the smaller one, with 36 SiO units. It is 0.05 eV/SiO less stable than structure **I**. This value is of the same (small) order as the enthalpy of formation of SiO_2 glass relative to α -quartz (experimental, 0.094 eV (9.1 kJ/mol);³⁷ computed, 0.083–0.10 eV (8–10 kJ/mol)³⁵). Given this difference in enthalpy, one might expect a crystalline form of SiO to persist over an amorphous one. However, the energy difference is not large, and with the variety of possible crystalline phases at $P = 1$ atm within a small enthalpy window (as discussed above), it is difficult to make such a prediction. A similar situation occurs in am- SiO_2 relative to quartz, yet both are known experimentally (as indicated above).

Five more models with 36 SiO units are close in energy to the enthalpically most stable one (less than 0.03 eV/SiO difference). The best larger model comprising 108 SiO units (216 atoms) is 0.018 eV/SiO less stable than the lowest energy amorphous model we found. However, since the larger approximant is a better representation of the real amorphous solid, it is taken as our primary (“best”) model for amorphous SiO (the smaller one is discussed in the SI). We will be referring to this best model ($Z = 108$) as sam- SiO (simulated amorphous SiO). The structure of the best amorphous SiO model is shown in Figure 5. The simulated radial distribution functions (rdf’s) and network statistics (see below) for this model are essentially identical to those for the smaller cell.

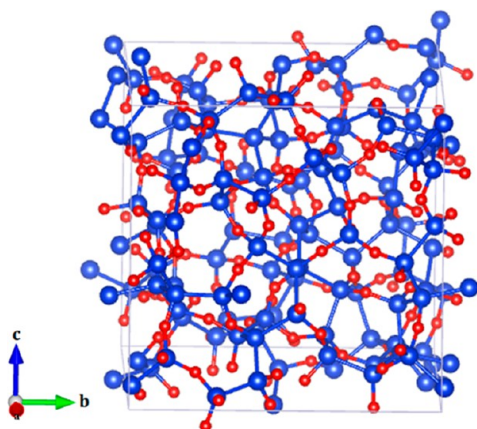


Figure 5. Ground-state structure of the best model of amorphous SiO ($Z = 108$) [blue = Si, red = O].

Structural information for amorphous SiO is accessible in principle from scattering probes sensitive to the two separate constituents, Si and O. These are, for example, anomalous X-ray diffraction and neutron scattering, which for appropriately large samples will yield the partial structure factors (the generalizations of the above for multicomponent systems), and for sufficiently large momentum transfers these in turn can yield via Fourier transformation the partial rdfs. We will show the experimental findings below.

Theoretically, the partial rdfs can be determined for amorphous systems by continuous approximations to discrete data resulting from methods which are also summarized below. Since the input to the latter also involves electronic density functional theory, the systems are formally to be regarded as crystalline but with finite unit cells (of approximate cell dimensions of 1.3 and 1.9 nm), where the finite bases are chosen to represent approximations to static amorphous structures. The aim is to obtain predictions of the equivalent of the partial rdfs obtained after the proposed averaging methods are applied. For completeness, links to the formal definitions of partial rdfs for binary systems are laid out in the Theoretical Section.

By way of a synopsis, the approach here to the approximate determination of partial rdfs, as outlined further in the Theoretical Section, is one based on determination for finite cells of the numbers of, say, SiO pairs (starting with a chosen Si atom for example) which are found within spherical shells at a prescribed separation from the atom, and also of a certain prescribed width. The ensuing tabulations are thus highly discrete, but are often made continuous by applying Gaussian broadening. From normalization procedures this process of averaging of what would normally take place for truly extended nondiffusive assemblies, and which may well take place via the extended nature of probe beams, leads to approximate estimates for the partial rdfs, as discussed below. These in turn offer certain insights into, for example, near-neighbor coordinations. The essential starting premise here is that the initial amorphous arrangements of SiO (these subsequently being optimized) may be obtained from the structure of vitreous phases of silica (SiO_2) by appropriate deletion of half of the oxygens.

In choosing the Gaussian width, we use a value which is found typical of theoretical studies³⁸ of macroscopic amorphous systems, both in elements and in compounds, namely 0.03 Å. Experimental values of the full width at half-

maximum (fwhm) are naturally greater for room-temperature measurements. With this broadening, we calculate the simulated partial and total rdfs for SiO as shown in Figure 6. The resulting average coordination of O around Si, Si around Si, and Si around O is 2.0.

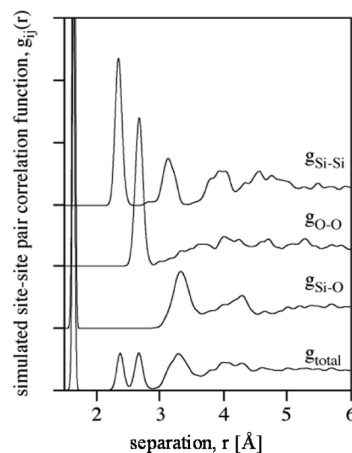


Figure 6. Simulated total and partial site-site pair correlation functions $g_{ij}(r)$ for the $Z = 108$ model of amorphous SiO. The curves are drawn to scale; the difference between two ticks on the ordinate is 3. All curves are normalized so that the averaged value is 1 at infinite separation. The maximum of the $g_{\text{Si-O}}$ curve is off-scale, at 40.9 (see discussion in text).

The first Si–O peak is located at 1.64 Å with a fwhm of 0.04 Å. It matches the typical Si–O bond distance that we compute for the various crystal structures of SiO (Table 2). The first Si–Si peak is located at 2.37 Å (fwhm = 0.12 Å) and is due to Si–Si bonds. It compares well with the Si–Si bond distance in the diamond structure of Si, for which we compute 2.37 Å. The first O–O peak is located at 2.66 Å (0.14 Å), arising from nonbonded O···O correlations within Si-centered tetrahedra. Additional pronounced peaks result from Si···Si correlations, at 2.84 Å (0.14 Å) arising from Si atoms connected via O and at 3.17 Å (0.21 Å) arising from Si at the corners of Si-centered tetrahedra. Another Si···O correlation is found at 3.3 Å (0.3 Å).

The very high and narrow first Si–O peak deserves further comment. Such high peaks might arise for crystals but are not typical for glasses, amorphous solids, or liquids. The first peak is so sharp because the simulated amorphous region is small (108 SiO units) and the Si–O bond so strong, short, and harmonic near its minimum; were the sample enlarged, the anharmonicity of the local bonding would be sampled, and the peak would broaden.³⁹ Experimentally, one observes very sharply defined local environments in silica (SiO_2).⁴⁰ Very large scale (300,000 atom models) simulations of SiO_2 also give a sharp first peak in the Si–O correlation at low temperatures.^{38,41}

The experimental partial pair correlation functions for amorphous SiO have, in fact, been investigated in the literature by combined X-ray, neutron, and electron diffraction techniques.^{7,42} The $g_{\text{SiSi}}(r)$ and $g_{\text{SiO}}(r)$ from this study are reproduced in Figure 7. The reported major Si–Si, Si–O, and O–O peaks lie at 2.45, 1.64, and 2.64 Å, quite comparable to the values obtained by us above (see Figure 6). One major discrepancy between our rdfs and those measured in ref 7 is in the second Si–O peak, at ~ 3.2 Å. This peak arises from Si–Si–O groupings, common in our structures. Hohl and co-workers note the absence of such a peak in their study and, in fact, take

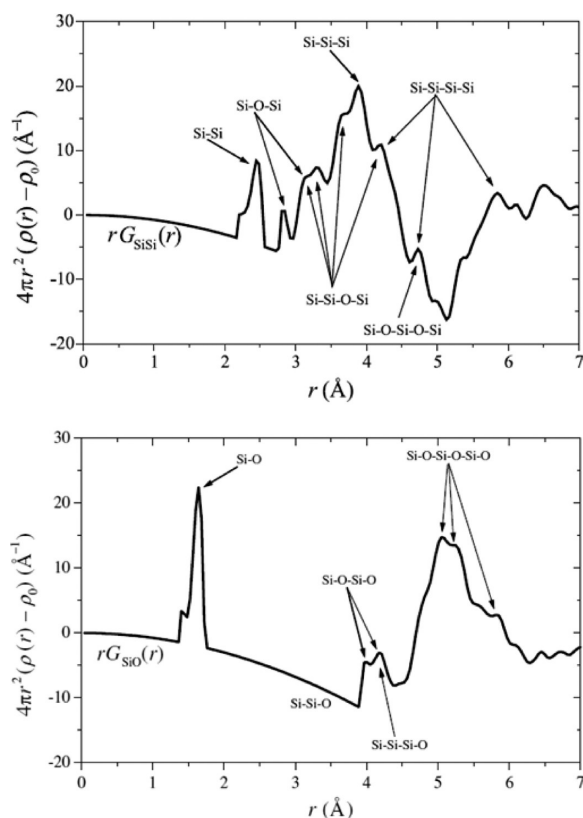


Figure 7. Experimental partial site–site pair correlation functions for Si–Si (top) and Si–O (bottom). Reproduced with permission from ref 7. Copyright 2003 Elsevier.

it as an indication of segregation of their SiO solid into SiO₂ and Si clusters (which would lack such a grouping).⁷ As mentioned above, our approximant to the amorphous phase does not show such segregation.

In Figure 8, we show the distribution of angles around Si and O atoms. It exhibits a maximum around a central Si angle of

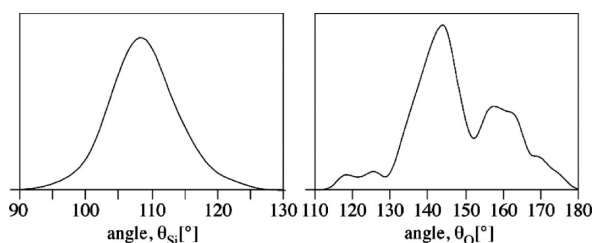


Figure 8. Angular distribution function for Si angles (left) and for the bond angle at O (for the $Z = 108$ sam-SiO model). The vertical axis is an arbitrary relative frequency of occurrence of a specified bond angle.

108.4° and an fwhm value of 11.2°. The angles at the O site are distributed between 120° and 180°, with one maximum at 143° and another one at 160°.

In the SI we show the simulated partial and total rdfs for two crystalline structures we found of lowest energy, structures I and II. In the short separation regime they do not differ much from the amorphous approximant—the first coordination sphere of Si and O is pretty well defined. Of course, at larger separations, the crystalline structures are much more “peaked” than the amorphous model.

Thus far, the structural data in terms of typical bond distances and angles do not distinguish a mixture of amorphous silica and silicon from a truly amorphous SiO. The two possibilities can be sorted out by looking at the coordination environment around the Si atoms: a segregated model will show an excess of {Si}O₄ and {Si}Si₄ tetrahedra at the expense of mixed tetrahedra, while a random model should follow proper random statistics.

In a random network, the probability of finding the coordination environments {Si}Si_nO_{4-n} ($n = 0, 1, 2, 3, 4$) is determined by the number of Si and O atoms and by their bonding in the system. If Si and O are 4- and 2-connected, respectively, and if no O–O bonds are present, then the total number of bonds N_{total} is given by $4/2N_{\text{Si}} + 2/2N_{\text{O}}$. The probability that a particular bond is an Si–O bond is $p(\text{Si–O}) = 2N_{\text{O}}/N_{\text{total}}$ and the probability that it is an Si–Si bond is $p(\text{Si–Si}) = 1 - p(\text{Si–O})$. In the case of a SiO₂ network this reduces to $p(\text{Si–O}) = 1$, while in a random network of SiO, $p(\text{Si–O}) = 2/3$ and $p(\text{Si–Si}) = 1/3$. It is indeed twice as likely to find a Si–O bond as it is to find a Si–Si bond; in our model with 36 units of SiO, we have in total 108 bonds, 72 of which are Si–O.

Each of the four neighbors of a Si atom can be either O or Si, with probability $p_{\text{TO}} = p(\text{Si–O})/[2p(\text{Si–Si}) + p(\text{Si–O})]$ for O and $p_{\text{TSi}} = 2p(\text{Si–Si})/[2p(\text{Si–Si}) + p(\text{Si–O})]$ for Si. The factor 2 in $2p(\text{Si–Si})$ arises because a Si can be on both ends of a Si–Si bond. Hence, in a random network of SiO, the probability of finding either O or Si around a central Si is equal.

Quantitatively, the probability $p(n)$ of finding the coordination environment {Si}Si_nO_{4-n} ($n = 0, 1, 2, 3, 4$) in a random SiO network is $p(n) = [4!/n!(4-n)!](p_{\text{TSi}})^n(p_{\text{TO}})^{4-n}$, with $p_{\text{TSi}} = p_{\text{TO}} = 0.5$. In our model comprising 108 units of SiO, we then expect 6.75, 27, 40.5, 27, and 6.75 for the numbers of {Si}Si_nO_{4-n} environments, and we find 3, 29, 46, 25, and 5, respectively. Given the relative statistical error ($1/\sqrt{N}$), the data are in agreement with a random network and, in particular, do not show a trend toward segregation of the structure into Si- and SiO₂-rich parts.

SiO Structures at Higher Pressures. The genetic algorithm that we employed to search for optimal structures led to several low-enthalpy ground-state structures for SiO under pressure. The search was performed at $P = 1$ atm and 10, 20, 50, 100, and 200 GPa (with different formula units Z ; see Theoretical Section for details). The resulting structures were then examined over a range of pressures. The enthalpically most stable phases above $P = 1$ atm are identified in the text using alphabetical symbols, as described in Table 4.

Figure 9 shows the relative enthalpy–pressure relation of these phases. The reference line is the enthalpically unstable SnO-type structure.^{45,46} Two of these structures have distinct

Table 4. Most Stable High-Pressure Ground-State Crystalline Phases of SiO

label ^a	space group	Z^b
A	$P2_1/m^{43}$	4
B	$Imm2^{44}$	4
C	$Imm2$	3
D	$P1-C2/m$	4
E	$C2/m$	4

^aThe alphabetical labels will be used in the text to identify these structures. ^b Z = number of formula units per unit cell.

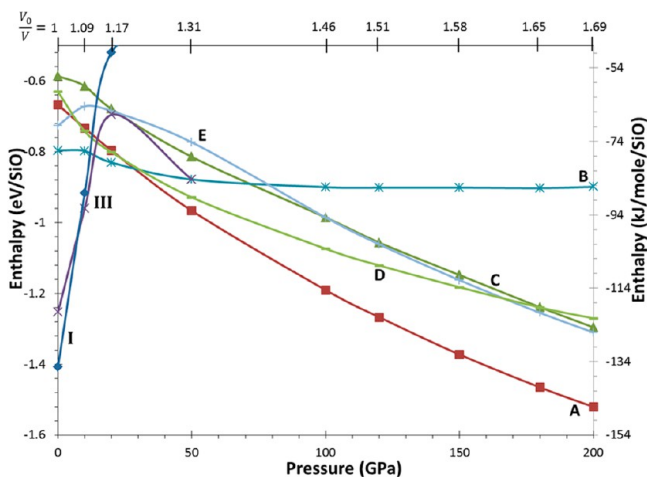


Figure 9. Enthalpy–pressure relation of the several potential static ground-state phases of solid SiO, relative to the SnO-type (tetragonal) structure. The zero enthalpy reference line is above the energy window of this graph. The volume compression of structure A up to 200 GPa is given on the top horizontal axis. V_0 is for structure A at $P = 1$ atm.

regions of overall stability: **B** is favored in a small pressure range between 10 and 30 GPa, while **A** is stable above 30 GPa. The $P = 1$ atm structures, **I** and **III**, are competitive only up to 10 GPa. Note that there is a small window of pressure, ~ 10 GPa, where structure **III** is favored enthalpically; at higher pressures, it transforms into **B** (around $P = 50$ GPa). No imaginary frequencies for the calculated phonons were found for the enthalpically stable structures **I**, **III**, **A**, and **B** at $P = 1$ atm, 10 GPa, 50 GPa, and 50 GPa, respectively, indicating their dynamic stability. The calculated phonon densities of states (DOSs) are reported in the SI. As mentioned above, the differences in enthalpy between many of the structures considered are comparable to the values of the ZPE (0.17 eV at $P = 1$ atm for **I**, 0.20 eV at $P = 50$ GPa for **A**). However, these structures have similar ZPEs, and we do not expect the ZPE to alter the structural choices.

Structure **A**, the most stable for $P \geq 30$ GPa, contains a ladder-like arrangement of extended Si units shown in Figure 10. These Si strips are connected with each other by distorted octahedral stishovite-like units. Bond lengths in **A** at 50 GPa are comparable to Si–Si in hexagonal-close-packed (hcp) silicon and Si–O in stishovite at the same pressure (Table 2). The Si–O–Si links that connect the stishovite-like units to the Si strips have angles of 126° and 129° , which are close to the angle found in the high-pressure SiO₂-stishovite, 131° (calculated). As expected, both Si and O atoms increase their coordination under pressure. Si tends to become 6-coordinated with increasing pressure, instead of the 4-coordination of $P = 1$ atm structures, while O tends to become 3- or 4-coordinated instead of 2-coordinated.

In a narrow intermediate pressure range we find **B** to be the most stable structure.⁴⁷ Interestingly, **B** contains in it elements of two structural types, stishovite-like SiO₂ units sandwiched between Si triangular nets. The structure of **B** at 50 GPa is shown in Figure 11. In this structure, Si–O and Si–Si bond lengths are 1.70–1.79 and 2.31–2.55 Å, respectively; these are similar to Si–O in the high-pressure quartz structure, stishovite, and Si–Si in hcp silicon at the same pressure (1.72 and 2.44 Å, respectively; see Table 2). Further, the Si–O and Si–Si interlayer distances are 1.72 and 2.43 Å, respectively. The

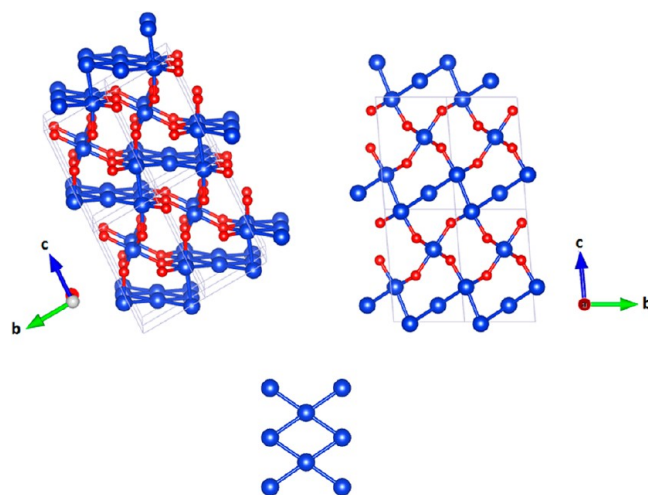


Figure 10. Static ground-state structure of **A** (see text) at $P = 50$ GPa (top). Si strips make up the ladder-like arrangement (bottom) [blue = Si, red = O].

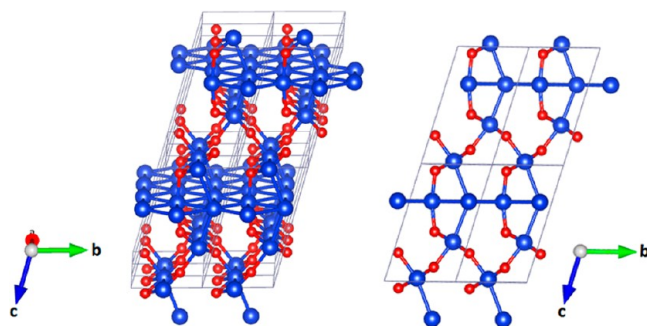


Figure 11. Static ground-state structure of **B** (see text) at 50 GPa in two views [blue = Si, red = O].

structure can be seen as incipiently segregated into Si and SiO₂ lattices. We will return to this possibility when we examine the energetics of the various structures relative to Si and SiO₂. However, the interlayer distances are short, and they indicate strong interaction between these two distinct regions. It is fascinating that **B** was obtained by applying pressure to the $P = 1$ atm phase, **III**; the Si chains and the α -quartz-like units in **III** have now transformed to Si triangular nets and stishovite-like units in **B**.

The structures of the other phases, **C**, **D**, and **E**, competing at intermediate pressures with **A** and **B**, are described in the SI.

But nothing is simple in the SiO system. In the range 0–20 GPa, the structure search produced several structures that are close in enthalpy to the most stable phases discussed above in the text. These phases have many common features, differing in some cases only by small deformations (their coordinates are given in the SI). In a sense it is then not surprising that amorphous forms of SiO will exist at low pressures, as is experimentally observed. In fact, an amorphous solid is not too far in enthalpy from our proposed ordered structures, as we discussed above.⁴⁸ The existence of a number of competing low-pressure structures is also not surprising, given the variety of silica polymorphs with their wide range of bond angles and bond lengths.²⁰ Similar to the SiO story, many of the known stable and metastable silica phases, differing only in the connectivity of their basic tetrahedral units, are close in enthalpy at low pressures.²⁰ At high pressures for both SiO and

SiO₂ there is a clearer enthalpic distinction among possible structures.

We have also examined the relative stability of structures A and C at $P = 100$ GPa using an LDA energy functional; A is still the most stable structure in that region. The relative enthalpies of these two structures using GGA-PBE and LDA calculations are compared in Table S4 in the SI.

Enthalpic Stability and Disproportionation. Up to this point, we have only considered the relative stability of the most stable phases with respect to each other. However, there are two main questions we need to address: How stable are these phases with respect to separation into the elements Si + O₂? And, perhaps more importantly, how stable are they with respect to disproportionation into Si + SiO₂? We calculated the heat of formation, Si_(s) + 1/2O_{2(s)} → SiO_(s), and the enthalpy of disproportionation, 2SiO_(s) → Si_(s) + SiO_{2(s)} for the various stable phases over a range of pressures.

Let us examine first the structures at $P = 1$ atm, where the competitive phases are I, II, and III, along with sam-SiO, as discussed above (*Cmcm* is shown for comparison). Table 5 gives the calculated heats of formation and disproportionation.

Table 5. Heats of Reaction for Si_(s) + 1/2O_{2(s)} → SiO_(s) (ΔH_f) and 2SiO_(s) → Si_(s) + SiO_{2(s)} (ΔH_{dis}) for the Most Stable Calculated Crystalline Ground-State Structures of SiO at $P = 1$ atm

phase	ΔH_f (kJ/mol)	ΔH_{dis} (kJ/mol)
<i>Cmcm</i>	-337 (-3.49 eV)	-157 (-1.63 eV)
I	-363 (-3.76 eV)	-83 (-0.86 eV)
II	-358 (-3.71 eV)	-93 (-0.96 eV)
III	-348 (-3.61 eV)	-113 (-1.17 eV)
am-SiO	-357 (-3.70 eV)	-96 (-0.995 eV)

Note the tremendous stabilization of the solid phase relative to the diatomic molecule, whose $\Delta H_f = -100$ kJ/mol (see Table 1). It follows that SiO is not behaving like CO at all, but much more like SnO and PbO, both forming extended solids with extremely different structures from the known diatomic molecules of the same stoichiometry. Solid SiO clearly has a large negative heat of formation; it is actually the largest in magnitude of all the group 14 monoxides.

How accurate are our results? First let us emphasize that the computed ΔH of disproportionation of am-SiO (-96 kJ/mol) compares well with experimental data (-65 kJ/mol, inferred from Table 1). While experimental errors are typical in the range of 20 kJ/mol,⁶ we estimate the computational error arising from modeling the amorphous structure to be of the same order.³⁵ The difference between our calculated ΔH_f^0 of am-SiO (-357 kJ/mol) and the carefully derived experimental ΔH_f^{298} (-423 kJ/mol⁶) is somewhat larger, but reflects more the difficulties of the theoretical method (DFT) comparing molecules and extended systems at the same time. Part of the difference derives from the correction needed to take a ΔH_f from 0 to 298 K (again O₂ is involved), but we estimate this as <10 kJ/mol.

Relative to quartz, SiO is thermodynamically unstable. The thermodynamic situation for SiO at $P = 1$ atm now resembles more closely that of the other monoxides of group 14; this is illustrated in Table 6, which shows the heats of disproportionation for the group, excluding GeO (unknown as a solid). Except for PbO,⁴⁹ all other monoxides have negative heats of disproportionation. Note the steady evolution of this heat down

Table 6. Heats of Disproportionation (ΔH_{dis} for 2EO → EO₂ + E) for Group 14 Monoxides except GeO at $P = 1$ atm^a

EO	ΔH_{dis} (kJ/mol)	notes
CO	-172 (-1.78 eV)	gas-phase experimental, 298 K ¹⁴
SiO	-83 (-0.86 eV)	ground-state theoretical value
SnO	-16 (-0.17 eV)	experimental, 298 K ¹⁷
PbO	+164 (1.70 eV)	experimental, 298 K ¹⁴

^aE = group 14 element. Si, Sn, and Pb systems are in the solid phase; C is in the gas phase.

the series, the way it changes from highly negative (CO) to highly positive (PbO).

It is quite remarkable that CO has a much greater tendency for disproportionation to CO₂ and C than does SiO into SiO₂ and Si. And yet we can have CO in a bottle. Even if the drive to disproportionation is greater for CO than for any group 14 monoxide, the activation energy for doing so is clearly larger in the carbon phase. This is, of course, a general phenomenon in carbon chemistry—for instance, in the presence of molecular oxygen all hydrocarbons are thermodynamically unstable; they burn! But the barriers to reaction with molecular oxygen are large. Organic chemistry is the land of the thermodynamically unstable but the kinetically persistent.

The moment one moves down group 14, the barriers to reaction (such as disproportionation) become smaller; why they do is something we will in time learn. The magnitudes of the negative ΔH_{dis} are decreasing down group 14 until they become positive (and large) for Pb.

Is SiO's thermodynamic tendency to disproportionate to Si and SiO₂ a barrier to it being made and persisting? That is, will crystalline SiO be kinetically persistent? It must be plainly admitted that we are unable, with the resources available to this group, to make an estimate of the kinetic persistence of SiO. As a reviewer has pointed out, arguing against the persistence of SiO is that the heat of reaction for dioxide formation from the monoxide, EO_(s) + 1/2O_{2(g)} → EO_{2(s)}, is greatest for group 14 when E = Si (see Table 1).

On the other hand, we are encouraged by the known persistence of CO and SnO (and by that of PbO₂, unstable with respect to PbO in the presence of elemental Pb, yet clearly around). The instability of SiO with respect to the dioxide is similar to that one finds for CO and SnO. We think one could reasonably expect that kinetically persistent ordered SiO solids can be made, if not at 1 atm, then at higher pressure.

What will in fact change for SiO as the pressure increases? Figure 12 shows the enthalpy of formation and disproportionation as a function of pressure for three of the calculated SiO phases. The high-pressure phases are clearly stable (these are ground-state calculations) with respect to separation into the elements up to 200 GPa. The $P = 1$ atm instability to disproportionation to Si + SiO₂ continues in the pressure regime investigated, increasing in magnitude at higher pressures. Unsurprisingly, SiO is thermodynamically unstable with respect to disproportionation at all pressures considered. And interestingly, there is a relative reduction in the magnitude of the disproportionation energy at low pressures, around 10 GPa.

As a geochemist, Mainak Mookherjee, has mentioned to us, there might have been special opportunity for SiO in the early stages of Earth's formation, when the atmosphere was oxygen-poor.

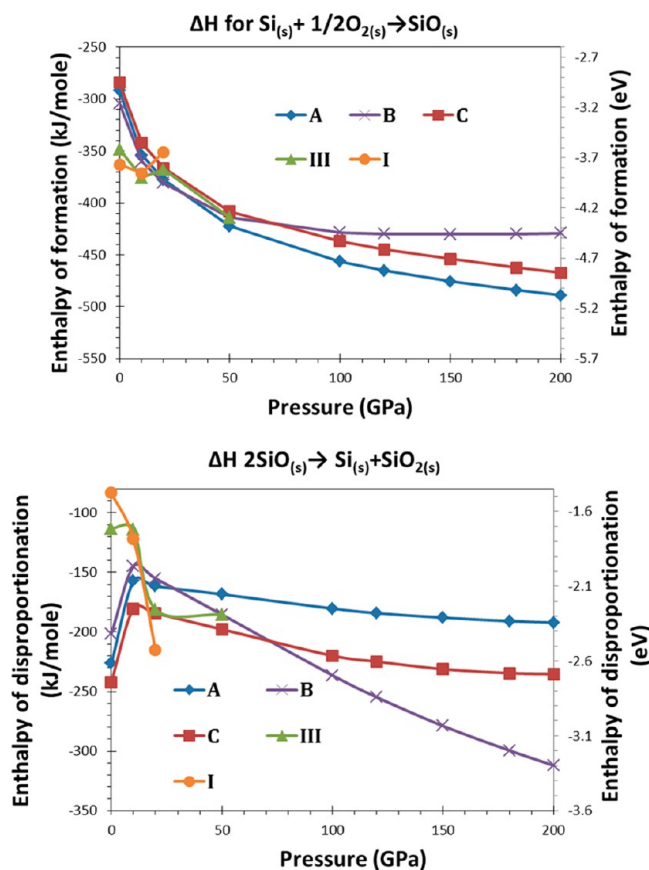


Figure 12. Static ground-state enthalpy of formation, $\text{Si}_{(s)} + 1/2\text{O}_{2(s)} \rightarrow \text{SiO}_{(s)}$ (top), and the enthalpy of disproportionation to SiO_2 of various SiO phases as a function of pressure, $2\text{SiO}_{(s)} \rightarrow \text{Si}_{(s)} + \text{SiO}_{2(s)}$ (bottom).

Electronic Structure of SiO. Figure 13, left side, shows the calculated electronic DOS per electron of structure I for SiO at $P = 1$ atm, compared to those of diamond-type silicon and α -quartz, also at 1 atm. The electronic structures of the other competitive $P = 1$ atm phases (reported in SI) are similar to that of I. Elemental silicon itself is a semiconductor, and its experimental 1.1 eV gap⁵⁰ is usually underestimated by the computation. SiO_2 is, of course, an insulator; in the extreme of an ionic viewpoint ($\text{Si}^{4+}(\text{O}^{2-})_2$), the oxygen bands are completely filled, opening a wide band gap between O [2p] and the unoccupied conduction band dominated by Si [3p] states. The real system, partially covalent, retains this ionic parentage—the conduction band is heavily Si 3p. The O 2s levels are near -19 eV (the zero of energy is the position of the highest occupied band, not the Fermi level); the Si 3s density is mainly in the region of -8 to -10 eV.

The electronic structure of SiO at $P = 1$ atm is understandably intermediate between those of Si and SiO_2 . It is similar to that of SiO_2 at $P = 1$ atm, except that in the former the valence band maximum has a substantial contribution of Si [3p] states, whereas in the latter they are O [2p] states. The presence of substantial Si 3p character above and below the highest occupied crystal orbital is due to the formation in SiO of Si–Si bonds, weaker than Si–O bonds. To help us understand the bonding, at the suggestion of a reviewer, we performed a Crystal Orbital Hamiltonian Population (COHP) analysis.⁵¹ COHP is a DOS weighted by the corresponding Hamiltonian matrix elements. It identifies energetically bonding

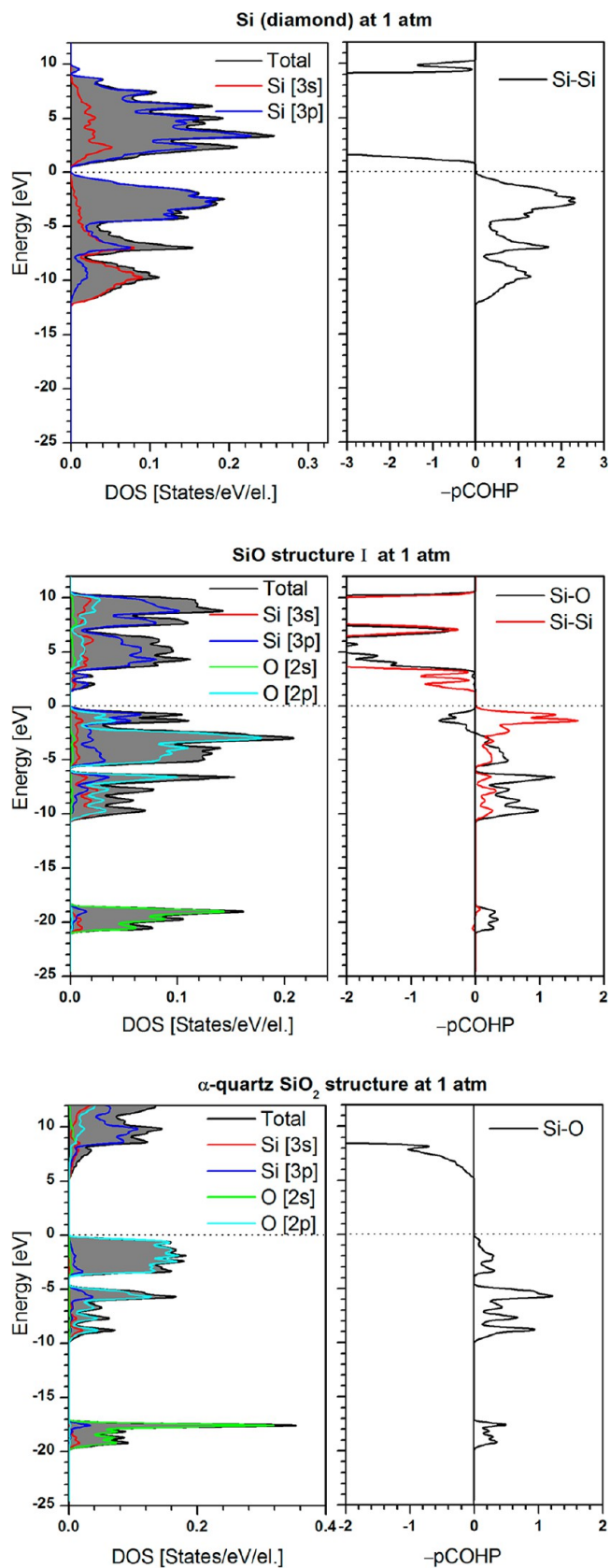


Figure 13. Electronic density of states of static, ground-state elemental Si-diamond, SiO (I), and α -quartz SiO_2 at $P = 1$ atm. The highest occupied energy level in the DOS is indicated with a dotted line. Next to each figure is a COHP plot (see text for description) indicating the bonding in the structure.

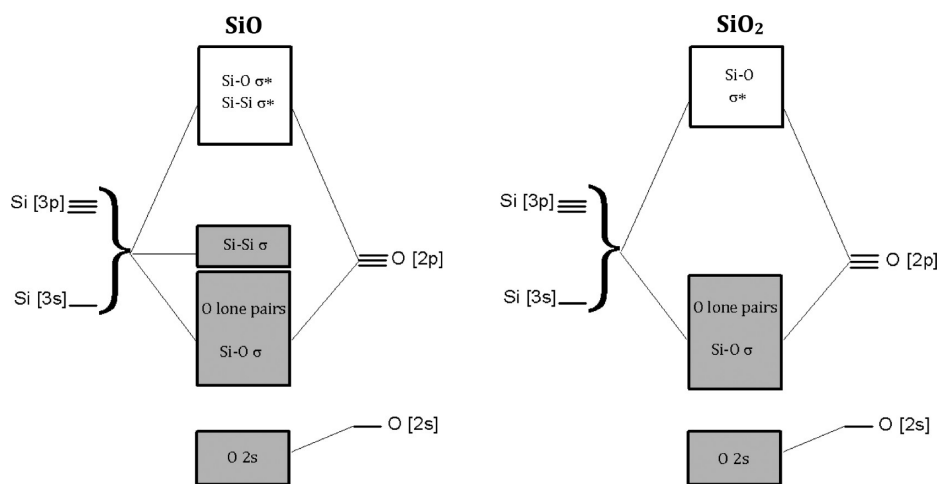


Figure 14. Schematic interaction diagrams for SiO (left) and SiO₂ (right). The “blocks” are representations for the DOSs presented for SiO and SiO₂. The filled levels are shaded in gray.

(and antibonding) components; a positive $-p\text{COHP}$ value indicates bonding, negative antibonding.

As the corresponding panels in Figure 13 show, in diamond Si all the occupied levels are Si–Si bonding, all unoccupied ones antibonding. In α -quartz, similarly, all the occupied levels are Si–O bonding, all unoccupied ones antibonding. But note (by comparing total DOS for α -quartz with the $-p\text{COHP}$) that the band of levels from 0 to -4 eV has a lot of states in it, but contributes little to Si–O bonding. These are the bridging O lone pairs (the projections in Figure 13 confirm this).

The SiO COHP analysis reveals one interesting feature: the states at the top of the valence band, between 0 and -4 eV, are actually Si–O antibonding. The levels in this region are primarily Si–Si bonding levels—note the strong Si–Si bonding in the COHP. But in a variant of hyperconjugation, antibonding σ^* levels of the Si–O bonds (four on average around each Si–Si bond in SiO) mix into these weak Si–Si bonds.

A schematic interaction diagram for SiO is compared with one for SiO₂ in Figure 14. The Si–O bond is strong, so the splitting between Si–O σ and σ^* levels is large. The Si–Si bond is weaker, so the Si–Si σ and σ^* splitting is smaller. The Si–Si and Si–O levels mix, as the COHP analyses and orbital projections of Figure 13 show, but this simplified scheme describes reasonably well the bonding in SiO.

An interesting comparison then emerges when we look at the calculated DOSs of the known group 14 monoxides at $P = 1$ atm along with structure I of SiO in Figure 15. The band gaps are underestimated because of the choice of functional and relativistic effects (in SnO and PbO) that we omitted. The known monoxides of the carbon group are all insulators at $P = 1$ atm. Note the “gapped” DOS for CO, typical of the molecular solid that it is.

Again, what happens as the pressure is increased? Figure 16 compares SiO at 1 atm and 50 GPa, where structure A is now metallic (structure B is also metallic; its electronic structure is shown in the SI). The metallicity of structure A can be attributed to (1) the inherent metallicity of the Si strips forming the Si sublattice [the Si–Si interaction in these strips is similar to that in hcp silicon, calculated to be metallic even at $P = 1$ atm] and (2) the fact that all the bands (O 2s, Si–O, Si–Si valence band) broaden under pressure [the metallization pressure of SiO is calculated to occur around 20 GPa (III-to-

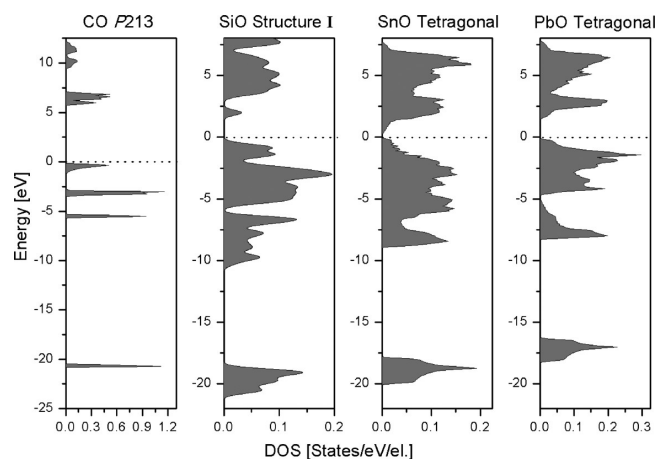


Figure 15. Calculated densities of electronic states, per electron, of the static ground-state structures of known group 14 monoxides along with the calculated SiO structure I at $P = 1$ atm. From left to right: CO solid in $P213$ structure, SiO structure I, SnO tetragonal, and PbO tetragonal.⁵² The dashed lines indicate the highest occupied levels.

B phase transition), which, as expected, is higher than that of elemental Si, around 10 GPa (cubic diamond to β -Sn structures)].²²

We note an increase of the silicon DOS near the eventual Fermi level with pressure. Integration of Si [3p] projected states between 0 and 2 eV in structure I and between 0 and 5 eV in structure A gives ~ 1 and 3 electrons, respectively. The DOS contributions add up to the total as shown; a Mulliken population analysis scheme as implemented in CASTEP⁵³ has been used to calculate the DOS (see SI for details).

CONCLUSION

We have presented the results of a computational study on potential stoichiometric and crystalline silicon monoxide, SiO, ground-state phases at $P = 1$ atm and at high pressures. The quest for stable SiO structures began with known and theoretical structures of group 14 monoxides, and continued with an evolutionary algorithm and random search procedures. As expected from silica (SiO₂), a number of structures were found to be stable for SiO at $P = 1$ atm; the enthalpically most stable of these was structure I (space group Cm).

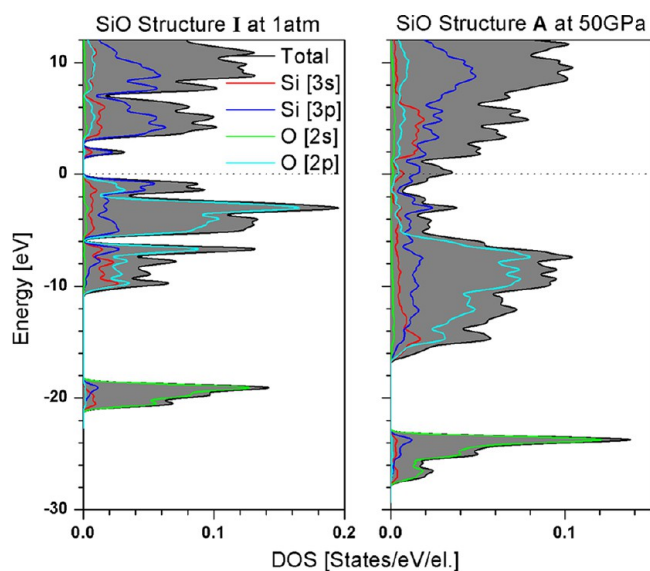


Figure 16. Electronic density of states per valence electron of static ground-state SiO structures I at $P = 1$ atm (left) and A at $P = 50$ GPa (right). The dashed line marks the energy zero, the highest occupied crystal orbital (and the Fermi energy in the 50 GPa case).

All these structures have some Si–Si bonds and quartz-like Si–O–Si linkages. At $P = 1$ atm, the lowest enthalpy SiO phases have four bonds to Si and two to O, with a range of Si–O–Si bond angles. Several approximants to amorphous SiO were also calculated. The best of these models comes out a little bit less stable than structure I and does not show segregation to SiO₂ and Si substructures. At higher pressures, three dynamically stable structures were found to have distinct regions of enthalpic stability: III, stable in a narrow pressure window between $P = 1$ atm and 10 GPa; B, stable between 10 and 30 GPa; and A, stable at higher pressures. At increased pressure (structures were studied up to 200 GPa), one begins to see higher coordinations of Si and O.

The best ground-state SiO structures have highly negative heats of formation. All the SiO phases are thermodynamically stable with respect to separation into the elements, but unstable with respect to disproportionation to Si and SiO₂. A common feature of the high-pressure phases is the formation of the inherently metallic Si strips and Si triangular nets. The electronic structure of these phases is intermediate between the known systems of SiO₂ and Si. Si–Si bonding in SiO leads to a small band gap in the $P = 1$ atm phases in comparison to α -SiO₂, and contributes to the metallic nature of the high-pressure phases of SiO.

THEORETICAL SECTION

All structures studied in this work were obtained from (1) known starting structures of relevant monoxide systems of group 14; (2) evolutionary structure search algorithms as implemented in XtalOpt program;⁵⁴ or (3) random structure search algorithms as implemented in AIRSS.⁵⁵

The structures of the group 14 monoxides were obtained from the Inorganic Crystal Structure Database (ICSD) and a recent theoretical work on solid carbon monoxide structures.¹³ The space groups of the structures that were investigated are listed below in Table 7.

The Vienna *ab initio* Simulation Package (VASP)⁵⁶ was applied to obtain the ground-state enthalpies of these structures, using density functional theory (DFT). The generalized gradient approximation of Perdew–Burke–Ernzerhof⁵⁷ was used as the energy functional in our calculations. The electron–ion interactions were treated by using the

Table 7. Group 14 Structures That Were Used as Starting Geometries for SiO

CO	theoretical: $P2_1/m$, $P2_1/c$, $Pbcm$, $P4/nmm$, $Pnma$, $I2_12_12_1$, $Cmcm$, $C2/m$, $C2/c$ experimental: $R3c$, $P2_13$
SnO	$P4/nmm$, $Cmc2_1$, $Pmn2_1$
PbO	$P4/nmm$, $Pbcm$

Projector Augmented Wave (PAW) method.^{58,59} The PAW pseudopotentials represent the valence electrons of Si ($3s^23p^2$) with a cutoff radius of 1.900 a_0 , and O ($2s^22p^4$) with a radius of 1.520 a_0 . A plane wave basis set cutoff of 600 eV/atom was set, and the structures were fully relaxed until the forces on the atoms were less than 10^{-3} eV/Å.

The structure search using XtalOpt was conducted at $P = 1$ atm ($Z = 4$), $P = 10$ GPa ($Z = 4, 3$), $P = 20$ GPa ($Z = 4$), $P = 50$ GPa ($Z = 2$), $P = 100$ GPa ($Z = 4, 3, 2$), and $P = 200$ GPa ($Z = 4$). The resulting structures were then examined over a range of pressures. Only ground-state calculations were performed in this work; ZPEs were not included. It is important to mention that the structure search performed at relatively low pressures (0–20 GPa) produced several structures that are close in enthalpy to the most stable phases discussed in the text. These phases have similar features to each other, with only small distortions in some cases. We report the coordinates of these phases in the SI.

Structure searches using AIRSS were carried out with four atoms ($2\text{Si} + 2\text{O}$) in the irreducible unit and up to four symmetry elements, as well as with eight atoms in the irreducible unit together with a single symmetry element. For each combination of cell content and symmetry elements, we generated at least 1000 structures. The searches were performed at ambient pressure and at 90 GPa.

The oxygen phases that were used to calculate the heats of formation and the heats of disproportionation for SiO structures are $C2/m$ at $P = 1$ atm, the ϵ O₂ phase between 10 and 50 GPa, and the ζ phase at higher pressures (100–200 GPa). Enthalpies of the various O₂ phases computed by us are consistent with what is reported in the literature on solid oxygen.^{21,60} The Si phases were cubic diamond at $P = 1$ atm, β -Sn at $P = 10$ GPa, $Imma$ at $P = 20$ GPa, hcp structure at $P = 50$ GPa, and face-centered cubic (fcc) at higher pressures, again with geometries and relative enthalpies as in the literature.²² The SiO₂ phases that were used to calculate the heats of disproportionation are α -quartz at $P = 1$ atm and stishovite at higher pressures.²⁰ The phonon calculations were carried out using PHONOPY code⁶¹ interfaced with VASP. Gaussian 09⁶² was used to optimize the (HO)₃-E-O-E-(OH)₃ model (E = Si, C). The DFT procedure used Becke's three-parameter hybrid functional, as modified by Lee, Yang, and Parr (B3LYP), and the split-valence 6-311++G (d,p) basis set. All space groups of the structures reported in this work were identified using FINDSYM program⁶³ and Spglib.⁶⁴

To set our simulation of rdf's in context, it may be useful to recall the essence of the origin and definition of the rdf for a homogeneous one-component atomic system which is both translationally and rotationally invariant, as for example in diffusive liquid or gaseous phases. Though its definition is not contingent on systems with solely pairwise interactions ($\varphi^{(2)}(r - r')$), its relation to these is especially informative. Consider a system of N such atoms in a volume V , both quantities being quite macroscopic, so that the system can be taken in a thermodynamic limit. At any instant, that is, for one particular configuration, the total interaction energy is then just one-half of a discrete sum over all possible distinct pairs at their momentary separations. As is well known, this can be immediately reformulated in terms of a double integral over continuous variables r and r' by the simple expedient of introducing the requisite delta-functions. It follows that for this single configuration, the potential energy of interaction is

$$\frac{1}{2} \int dr \int dr' \varphi^{(2)}(r - r') \rho^{(2)}(r, r')$$

where $\rho^{(2)}(r - r')$ is now the two-particle density operator. It is clear that in any ensuing statistical averaging, for example over the

developing configurations of a liquid, it is the quantity $\rho^{(2)}(r-r')$ that will be averaged. The result is then a two-particle density, and for a homogeneous system it too is just a function of the relative variable $r-r'$.⁶⁵

However, on the matter of averaging, there is an important point (and one that is distinctly different for noncrystalline states that are nondiffusive); it may be introduced this way: At any instant, for a fluid, the prescribed macroscopic volume can itself be regarded as a large assembly of subvolumes, each plausibly in its own thermodynamic limit. The well-known consequence of this is that these subvolumes provide a basis for executing both translational and rotational averaging so that the single configuration of the originating grand assembly actually suffices to define a rdf and associated static structure factor of the corresponding homogeneous and diffusive liquid occupying one of the subvolumes. The ensuing rdf has a precise statistical interpretation for the liquid or gaseous state; given a particle at the origin, it is the probability of finding another at separation r in the presence of correlations but relative to the same quantity in the absence of such correlations. In practical situations for liquids it is also determined, of course, from simulations carried out on finite systems, but (and here again arises the important difference) for a multitude of different configurations.

It is quite clear that similar arguments could be invoked in principle for a large noncrystalline but nondiffusive system. But there is a quite crucial proviso: it is that sufficient structural information is available for the assembly of subvolumes, each required, as in the above to be in a reasonable thermodynamic limit. This, of course, is a nontrivial requirement and is presently not achievable. For clear computational reasons, treatments of amorphous systems have limited particle numbers, and the cells used for them (see above) are also quite limited in size; only a single configuration is available, and this is not subsequently averaged by the procedures available for liquids. This has led to a different approach to the approximate determination of partial rdfs, as outlined below.

For simulating the amorphous model of SiO, simulated site–site pair correlation functions $g(r)$ were generated by counting the number of nearest neighbors between distances r and $r+\Delta r$ around an atom center (we use $\Delta r = 0.1$ Å). While the total site–site pair correlation function accumulates distance correlations between all atoms (as center as well as as neighbor at distance r), the partial pair correlation function does this for particular pairs (e.g., from center Si to neighbor O) specifically. All individual entries of distance between two sites are convoluted with a normed Gaussian function with a fwhm of 0.03 Å (0.10 Å for distances above 2.3 Å) and subsequently averaged and normed by the neighbor number density expected for this distance. Through this construction, all simulated site–site pair correlation functions yield an average value of 1 at infinite separation. Angular distributions were generated by broadening individual entries of angles around a specific site (108 for O, 432 for Si) by Gaussian functions with a fwhm of 5°.

■ ASSOCIATED CONTENT

📄 Supporting Information

Discussion of several structures that were not analyzed in the main text; geometries of the structures discussed (in addition to others); phonon DOSs; electronic band structures for structures A and B; band gaps for the $P = 1$ atm structures; and discussion of a high-pressure insulating phase. This material is available free of charge via the Internet at <http://pubs.acs.org>.

■ AUTHOR INFORMATION

Corresponding Author

rh34@cornell.edu

Present Address

#Department of Chemistry, Indian Institute of Technology, Kanpur 208016, India.

Notes

The authors declare no competing financial interest.

■ ACKNOWLEDGMENTS

We thank Saudi Aramco for supporting K.A. in pursuing his degree. Our work at Cornell was supported by NSF Research Grant CHE-0910623 and DMR-0907425. Work at U. Texas at Arlington was supported by NSF Research Grant DMR-0907117. Computational facilities provided by KAUST (King Abdullah University of Science and Technology) Supercomputing Laboratory, EFree (an Energy Frontier Research Center funded by the Department of Energy, award no. DEC0001057 at Cornell), the XSEDE network (provided by the National Center for Supercomputer Applications through Grant TG-DMR060055N), the IIT Kanpur Computer Centre High Performance Computing facility, and Cornell's NanoScale Facility (supported by the National Science Foundation through Grant ECS-0335765) are gratefully acknowledged. We thank Andreas Hermann for useful discussions.

■ REFERENCES

- (1) Kuwayama, Y.; Hirose, K.; Sata, N.; Ohishi, Y. *Science* **2005**, *309*, 923.
- (2) Tsuchiya, T.; Tsuchiya, J. *Proc. Natl. Acad. Sci. U.S.A.* **2011**, *108*, 1252.
- (3) Prakapenka, V. P.; Shen, G.; Dubrovinsky, L. S.; Rivers, M. L.; Sutton, S. R. *J. Phys. Chem. Solids* **2004**, *65*, 1537.
- (4) Ferguson, F. T.; Nuth, J. A., III *J. Chem. Eng. Data* **2008**, *53*, 2824.
- (5) Kim, J.-H.; Park, C.-M.; Kim, H.; Kim, Y.-J.; Sohn, H.-J. *J. Electroanal. Chem.* **2011**, *661*, 245.
- (6) Schnurre, S. M.; Gröbner, J.; Schmid-Fetzer, R. *J. Non-Cryst. Solids* **2004**, *336*, 1.
- (7) Hohl, A.; Wieder, T.; van Aken, P. A.; Weirich, T. E.; Denninger, G.; Vidal, M.; Oswald, S.; Deneke, C.; Mayer, J.; Fuess, H. *J. Non-Cryst. Solids* **2003**, *320*, 255.
- (8) Cherchneff, I. *EAS Publ. Ser.* **2013**, *60*, 175.
- (9) Schnöckel, H.; Köppe, R. Reactions with Matrix Isolated SiO Molecules. In *Silicon chemistry: from the atom to extended systems*; Jutz, P., Schubert, U., Eds.; Wiley-VCH GmbH & Co. GaA: Weinheim, 2003; p 28.
- (10) McCarthy, M. C.; Gottlieb, C. A.; Thaddeus, P. *Mol. Phys.* **2003**, *101*, 697.
- (11) Wang, H.; Sun, J.; Lu, W. C.; Li, Z. S.; Sun, C. C.; Wang, C. Z.; Ho, K. M. *J. Phys. Chem. C* **2008**, *112*, 7097 and references therein.
- (12) Schnöckel, H. and Köppe, R. Reactions with Matrix Isolated SiO molecules. In *Silicon chemistry: from the atom to extended systems*; Jutz, P., Schubert, U., Eds.; Wiley-VCH GmbH & Co. GaA: Weinheim, 2003; p 20.
- (13) Sun, J.; Klug, D. D.; Pickard, C. J.; Needs, R. *Phys. Rev. Lett.* **2011**, *106*, 145502.
- (14) Chase, M. W., Jr. NIST-JANAF Thermochemical Tables, 4th ed. *J. Phys. Chem. Ref. Data* **1998**, Monograph 9, 1.
- (15) Luo, Y.-R. BDEs of Si-, Ge-, Sn-, and Pb-X bonds. In *Comprehensive Handbook of Chemical Bond Energies*; Taylor and Francis Group: New York, 2007; p 472.
- (16) The ΔH_f value was calculated using the formula $\Delta H_f(\text{GeO}) = \Delta H_f(\text{O}) + \Delta H_f(\text{Ge}) - \text{BDE}(\text{GeO})$, all in the gas phase. BDE is the bond dissociation energy obtained from ref 15.
- (17) Cox, J. D.; Wagman, D. D.; Medvedev, V. A. *CODATA Key Values for Thermodynamics*; Hemisphere Publishing Corp.: New York, 1984; p 1.
- (18) Mankefors, S.; Andersson, T. G.; Panas, I. *Chem. Phys. Lett.* **2000**, *322*, 166.
- (19) Jenkins, S. *J. Phys.: Condens. Matter* **2002**, *14*, 10251.
- (20) Demuth, T.; Jeanvoine, Y.; Ángyán, J. G. *J. Phys.: Condens. Matter* **1999**, *11*, 3833.

- (21) Kim, D. Y.; Lebègue, S.; Araújo, M.; Arnaud, B.; Alouani, M.; Ahuja, R. *Phys. Rev. B* **2008**, *77*, 092104.
- (22) Mujica, A.; Rubio, A.; Munoz, A.; Needs, R. J. *Rev. Mod. Phys.* **2003**, *75*, 863.
- (23) Walsh, R. *Acc. Chem. Res.* **1981**, *14*, 246.
- (24) Walsh, R. Thermochemistry. In *The Chemistry of Organic Silicon Compounds*; Patai, S., Rappoport, Z., Eds.; John Wiley and Sons Ltd.: Chichester, 1989; Vol. 1, Part 1, pp 371–391.
- (25) Becerra, R.; Walsh, R. Thermochemistry. In *The Chemistry of Organic Silicon Compounds*; Rappoport, Z., Apeloig, Y., Eds.; John Wiley and Sons Ltd.: Chichester, 1998; Vol. 2, Part 1, pp 152–180.
- (26) Hubbard, C. R.; Swanson, H. E.; Mauer, F. A. J. *Appl. Crystallogr.* **1975**, *8*, 45.
- (27) Ogata, K.; Takeuchi, Y.; Kudoh, Y. *Z. Kristallogr.* **1987**, *179*, 403.
- (28) (a) Apeloig, Y. Theoretical aspects of organosilicon compounds. In *The Chemistry of Organic Silicon Compounds*; Patai, S., Rappoport, Z., Eds.; John Wiley and Sons Ltd.: Chichester, 1989; Vol. 1, Part 1, pp 57–225. (b) Karni, M.; Kapp, J.; Schleyer, P. v. R.; Apeloig, Y. Theoretical aspects of compounds containing Si, Ge, Sn and Pb. In *The Chemistry of Organic Silicon Compounds*; Rappoport, Z., Apeloig, Y., Eds.; John Wiley and Sons Ltd.: Chichester, 2001; Vol. 3, pp 1–163.
- (29) Similar calculations have been reported: (a) Oganov, A.; Ono, S.; Yanming, M.; Glass, C.; Garcia, A. *Earth Planet. Sci. Lett.* **2008**, *273*, 38. (b) Lasaga, A.; Gibbs, G. V. *Phys. Chem. Miner.* **1988**, *16*, 29. (c) See also Dawson, C. J.; Sanchez-Smith, R.; Rez, P.; O’Keeffe, M.; Treacy, M. J. *Chem. Mater.* **2014**, in press.
- (30) Weinhold, F.; West, R. *Organometallics* **2011**, *30*, 5815.
- (31) The structure search scheme that we employed did not predict Cmc_m.
- (32) Hirose, T.; Kihara, K.; Okuno, M.; Fujinami, S.; Shinoda, K. *J. Mineral. Petrol. Sci.* **2005**, *100*, 55.
- (33) Glinnemann, J.; King, H. E., Jr.; Schulz, H.; Hahn, Th.; La Placa, S. J.; Dacol, F. Z. *Kristallogr.* **1992**, *198*, 177.
- (34) Wooten, F.; Winer, K.; Weaire, D. *Phys. Rev. Lett.* **1985**, *54*, 1392.
- (35) (a) Kroll, P. *J. Mater. Chem.* **2003**, *13*, 1657. (b) Charpentier, Th.; Kroll, P.; Mauri, F. *J. Phys. Chem. C* **2009**, *113*, 7917. (c) Kroll, P. *J. Mater. Chem.* **2010**, *20*, 10528.
- (36) Kroll, P. In *Ceramics Science and Technology*; Riedel, R., Chen, L.-W., Eds.; Wiley-VCH: New York, 2008; Vol. 1, p 41.
- (37) (a) Petrovic, I.; Navrotsky, A.; Davis, M. E.; Zones, S. I. *Chem. Mater.* **1993**, *5*, 1805. (b) Hu, Y. T.; Navrotsky, A.; Chen, C. Y.; Davis, M. E. *Chem. Mater.* **1995**, *7*, 1816.
- (38) For silicon, we found two good simulations, but neither gives the fwhm assumed directly. However, one gives the rdf for crystalline Si, and the fwhm of the first peak (~2.38 Å), and then presumably gives us the assumed fwhm of their model: Stillinger, F. H.; Weber, T. *Phys. Rev. B* **1985**, *31*, 5262. This fwhm is estimated by us—inaccurately, as this has to be done by enlarging the journal graphs and physically measuring the width—as 0.13 Å. The liquid form (simulated in this paper by 216 atoms) has naturally a larger fwhm of 0.29 Å. A second simulation of Si has been reported: Car, R.; Parinello, M. *Phys. Rev. Lett.* **1988**, *60*, 204. That paper says that the theoretical rdf for Si is sharper than the experimental one in the first peak; the authors then scale the simulation to compare with experiment for Ge, obtaining an fwhm which we estimate from their graph as 0.30 Å. The best experimental value we have found was reported here: Laaziri, K.; Kycia, S.; Roorda, S.; Chicoine, M.; Robertson, J. L.; Wang, J.; Moss, S. C. *Phys. Rev. Lett.* **1999**, *82*, 3460. From their rdf graph, our estimate of the experimental fwhm is 0.20 Å. For SiO₂, the first peak is at 1.60 Å, and is in theory and experiment much sharper than for crystalline or amorphous Si, because the Si–O bond is so strong. From a critical review of experimental data (Wright, A. C. *J. Non-Cryst. Solids* **1994**, *179*, 84), our estimate from the best data (neutron diffraction, Figure 14 of that paper) is that the fwhm is 0.075 Å. There are innumerable theoretical studies of the system, all of them using some broadening function, but almost never specifying it. However, we found one comprehensive study of models containing 60,000 and 300,000 atoms (!), using a Monte Carlo procedure at several temperatures: Vink, R. L. C.; Barkema, G. T. *Phys. Rev. B* **2003**, *67*, 245201. The results are fitted to Gaussian distributions with and without Fourier broadening, at several temperatures. At “0 K” the fwhm is 0.026 Å without Fourier broadening, and with Fourier broadening it is 0.113 Å. These are incredibly sharp peaks.
- (39) See, *inter alia*, for amorphous silicon and silica: de Graff, A. M. R.; Thorpe, M. F. *Acta Crystallogr. A* **2010**, *66*, 22.
- (40) Wright, A. C. *J. Non-Cryst. Solids* **1994**, *179*, 84.
- (41) See, in particular, Figure 2 in the following paper: Vink, R. L. C.; Barkema, G. T. *Phys. Rev. B* **2003**, *67*, 245201.
- (42) Earlier measurements of the total correlation functions can be found in the following: (a) Yasaitis, J. A.; Kaplow, R. *J. Appl. Phys.* **1972**, *43*, 995. (b) Temkin, R. J. *J. Non-Cryst. Solids* **1975**, *17*, 215.
- (43) At $P \leq 20$ GPa, the symmetry of this structure is *Pm*.
- (44) The symmetry of the B phase at $P = 1$ atm changes to *Cm* when decompressed from higher pressure.
- (45) For the high-pressure comparison we use the “ideal” SnO-type structure, which is 0.3 eV/SiO above the distorted SnO-type structure at $P = 1$ atm (the distorted structure was fully relaxed without any symmetry constraints).
- (46) The $P = 1$ atm structures that were obtained from the structure search quickly destabilize and then undergo phase transitions with pressure. Some of the new resulting phases were used to obtain some of the high-pressure phases discussed in the text. Upon decompression, these phases did not go back to the initial geometries.
- (47) Although structure B has a small range of stability and there are several structures competing with it (reported in the text or SI) in that small range, B shows structural features that are present in many of these competing phases that we found.
- (48) The same argument—availability of a manifold of competitive crystal structures—is used to explain the resistance of B₂O₃ to crystallization: Ferlat, G.; Seitsonen, A. P.; Lazzeri, M.; Mauri, F. *Nat. Mater.* **2012**, *11*, 925.
- (49) Ahuja, R.; Blomqvist, A.; Larsson, P.; Pyykkö, P.; Zaleski-Ejgierd, P. *Phys. Rev. Lett.* **2011**, *106*, 018301.
- (50) Yoshikawa, A.; Matsunami, H.; Nanishi, Y. In *Wide bandgap semiconductors: fundamental properties and modern photonic and electronic devices*; Takahashi, K., Yoshikawa, A., Sandhu, A., Eds.; Springer: Berlin, 2007; pp 11–23.
- (51) (a) COHP definition: Dronskowski, R.; Blöchl, P. E. *J. Phys. Chem.* **1993**, *97*, 8617–8624. (b) Projected COHP definition: Deringer, V. L.; Tchougréeff, A. L.; Dronskowski, R. *J. Phys. Chem. A* **2011**, *115*, 5461–5466. (c) See <http://www.cohp.de/>; COHPs were constructed from VASP input, using the LOBSTER software: Maintz, S.; Deringer, V. L.; Tchougréeff, A. L.; Dronskowski, R. *J. Comput. Chem.* **2013**, *34*, 2557–2567.
- (52) The total DOS of structure I is calculated using CASTEP, for consistency, the others using VASP.
- (53) Clark, S. J.; Segall, M. D.; Pickard, C. J.; Hasnip, P. J.; Probert, M. J.; Refson, K.; Payne, M. C. *Z. Kristallogr.* **2005**, *220*, 567.
- (54) Lonie, D. C.; Zurek, E. *Comput. Phys. Commun.* **2011**, *182*, 372.
- (55) Pickard, C. J.; Needs, R. J. *J. Phys.: Condens. Matter* **2011**, *23*, 053201.
- (56) Kresse, G.; Furthmüller, J. *Phys. Rev. B* **1996**, *54*, 11169.
- (57) Perdew, J. P.; Burke, K.; Ernzerhof, M. *Phys. Rev. Lett.* **1996**, *77*, 3865.
- (58) Blöchl, P. E. *Phys. Rev. B* **1994**, *50*, 17953.
- (59) Kresse, G.; Joubert, D. *Phys. Rev. B* **1999**, *59*, 1758.
- (60) We only considered the enthalpy of the C2/m (α) phase at $P = 1$ atm.
- (61) (a) Togo, A.; Oba, F.; Tanaka, I. *Phys. Rev. B* **2008**, *78*, 134106. (b) Baroni, S.; Gironcoli, S. D.; Corso, A. D.; Giannozzi, P. *Rev. Mod. Phys.* **2001**, *73*, 515.
- (62) Frisch, M. J.; Trucks, G. W.; Schlegel, H. B.; Scuseria, G. E.; Robb, M. A.; Cheeseman, J. R.; Scalmani, G.; Barone, V.; Mennucci, B.; Petersson, G. A.; Nakatsuji, H.; Caricato, M.; Li, X.; Hratchian, H. P.; Izmaylov, A. F.; Bloino, J.; Zheng, G.; Sonnenberg, J. L.; Hada, M.; Ehara, M.; Toyota, K.; Fukuda, R.; Hasegawa, J.; Ishida, M.; Nakajima, T.; Honda, Y.; Kitao, O.; Nakai, H.; Vreven, T.; Montgomery, J. A., Jr.;

Peralta, J. E.; Ogliaro, F.; Bearpark, M.; Heyd, J. J.; Brothers, E.; Kudin, K. N.; Staroverov, V. N.; Kobayashi, R.; Normand, J.; Raghavachari, K.; Rendell, A.; Burant, J. C.; Iyengar, S. S.; Tomasi, J.; Cossi, M.; Rega, N.; Millam, J. M.; Klene, M.; Knox, J. E.; Cross, J. B.; Bakken, V.; Adamo, C.; Jaramillo, J.; Gomperts, R.; Stratmann, R. E.; Yazyev, O.; Austin, A. J.; Cammi, R.; Pomelli, C.; Ochterski, J. W.; Martin, R. L.; Morokuma, K.; Zakrzewski, V. G.; Voth, G. A.; Salvador, P.; Dannenberg, J. J.; Dapprich, S.; Daniels, A. D.; Farkas, O.; Foresman, J. B.; Ortiz, J. V.; Cioslowski, J.; Fox, D. J. *Gaussian 09*, Revision A.02; Gaussian, Inc.: Wallingford, CT, 2009.

(63) Stokes, H. T.; Hatch, D. M. *J. Appl. Crystallogr.* **2005**, *38*, 237.

(64) Togo, A., <http://spglib.sourceforge.net/>.

(65) Ashcroft, N. W. Structure and Properties. In *Condensed Matter Physics*; Mahanty, J., Das, M. P., Eds.; World Scientific: Singapore, 1989; pp 1–70. McCarly, J. S.; Ashcroft, N. W. *Phys. Rev. E* **1997**, *55*, 4990.